ELSEVIER

Journal of Alloys and Compounds 312 (2000) 60–67

Journal of ALLOYS AND COMPOUNDS

www.elsevier.com/locate/jallcom

Dehydrogenation properties of nano-/amorphous Mg_2NiH_x by hydrogen induced mechanical alloying

Tae-Whan Hong, Shae-Kwang Kim, Young-Jig Kim*

School of Metallurgical and Materials Engineering, Sung Kyun Kwan University, 300 Chunchun-dong, Jangan-gu, Suwon, Kyunggi-do 440-746, South Korea

Received 18 April 2000; accepted 13 July 2000

Abstract

In recent years, nanocrystalline materials have been of interest for hydrogen storage applications. Especially, the great improvement of the hydrogenation properties of Mg alloys that can be achieved by nanocrystallization. In this study, nanocrystalline Mg_2NiH_x is fabricated from Mg and Ni chips by hydrogen induced mechanical alloying (MA) for 96 h under a high-pressure hydrogen atmosphere. The balls to chips mass ratios (BCR) are 30:1 and 66:1. The particles obtained are characterized by XRD and TEM, and absorbed hydrogen contents (AHC) were measured by TGA. For dehydrogenation kinetics, activation energies are calculated by isothermal thermogravimetry analysis (ITGA) and pressure–composition-isotherm (PCI) analysis. The results of XRD and TEM revealed that the Mg_2NiH_x peaks are broadened in the case of high BCR and the particles are composed of the nanocrystalline phases less than 10 nm with the amorphous phase. The results of ITGA and PCI analysis show that the dehydrogenation kinetics are greatly improved by nanocrystallization. The results show that BCR conditions mainly affect the size and fraction of the nanocrystalline phases, the resultant AHC and the dehydrogenation kinetics. © 2000 Elsevier Science B.V. All rights reserved.

Keywords: Amorphous materials; Mechanical alloying; X-ray diffraction; Hydrogen storage materials

1. Introduction

Nanocrystalline structure was defined as a new solid state as reported by Gleiter and co-workers. If the grain size is reduced to 10 nm or less, the density of the grain boundaries increases to 10^{18}~$10^{21}/cm^3$. This means that about 50% of the atoms are located in the grain boundaries. In other words, nanocrystalline structure can be regarded as a structural compound, one half of which consists of a crystalline phase and the other half of a grain boundary phase. This state entails considerable changes in the intrinsic material properties. In nanocrystalline materials, self-diffusion is enhanced by the factor of 10^{19} compared with conventional polycrystalline materials. The reason for this is the considerable density and the high cleanliness of the grain boundaries, which is in contrast to normal materials where the grain boundaries are to some extent filled up by segregation. In this regard, nanocrystalline materials are one of the best candidates for hydrogen storage [1–3].

On the other hand, magnesium and magnesium alloys are attractive materials for hydrogen storage applications, but activation, hydrogenation/dehydrogenation kinetics, thermodynamic equilibrium parameters and degradation behaviors have to be improved for applications [4]. Recently, crystal structure modification of the nanocrystalline structure with amorphous phases has been considered as one of the methods for improving the kinetic properties of the Mg and Mg alloys which experience problems with high desorption temperature and degradation phenomena. Especially, in the case of Mg based hydrogen storage intermetallic compounds, the nanocrystalline particles of Mg_2Ni with a grain size of less than 100 nm have been synthesized by mechanical alloying (MA) for improving the hydrogenation properties. The nanocrystalline particles shows a much easier activation compared with their conventional polycrystalline counterparts, mainly due to the nanocrystalline and amorphous phases with a variety of interstices available for hydrogen behaviors [5–10].

*Corresponding author. Tel.: +82-31-290-7357; fax: +82-31-290-7371.

E-mail address: yjk1122@yurim.skku.ac.kr (Y.-J. Kim).

0925-8388/00/$ – see front matter © 2000 Elsevier Science B.V. All rights reserved.
PII: S0925-8388(00)01131-2

In previous studies [11,12], hydrogen induced mechanical alloying was proposed using Mg and Ni chips to fabricate the nanocrystalline Mg_2NiH_x particles with the amorphous phases. In this paper, the dehydrogenation properties of the Mg_2NiH_x particles were characterized by isothermal thermogravimetry analysis (ITGA) and the fully hydrogenation behaviors by automatic pressure–composition-isotherm (PCI) analysis without activation. On the basis of our results, we intended to optimize the MA conditions.

2. Experimental methods

2.1. Fabrication and structure analysis of Mg_2NiH_x

Mg and Ni chips were prepared by drilling, without cutting oil, Mg (99.93%) and Ni (99.92%) ingots [Fig. 1(a)]. The initial chips (Mg–55 mass%Ni, 6 g) were charged in an AISI 304 jar, designed for high pressure operation and equipped with needle valves for evacuating air and introducing hydrogen gas. The jar of 450 cc

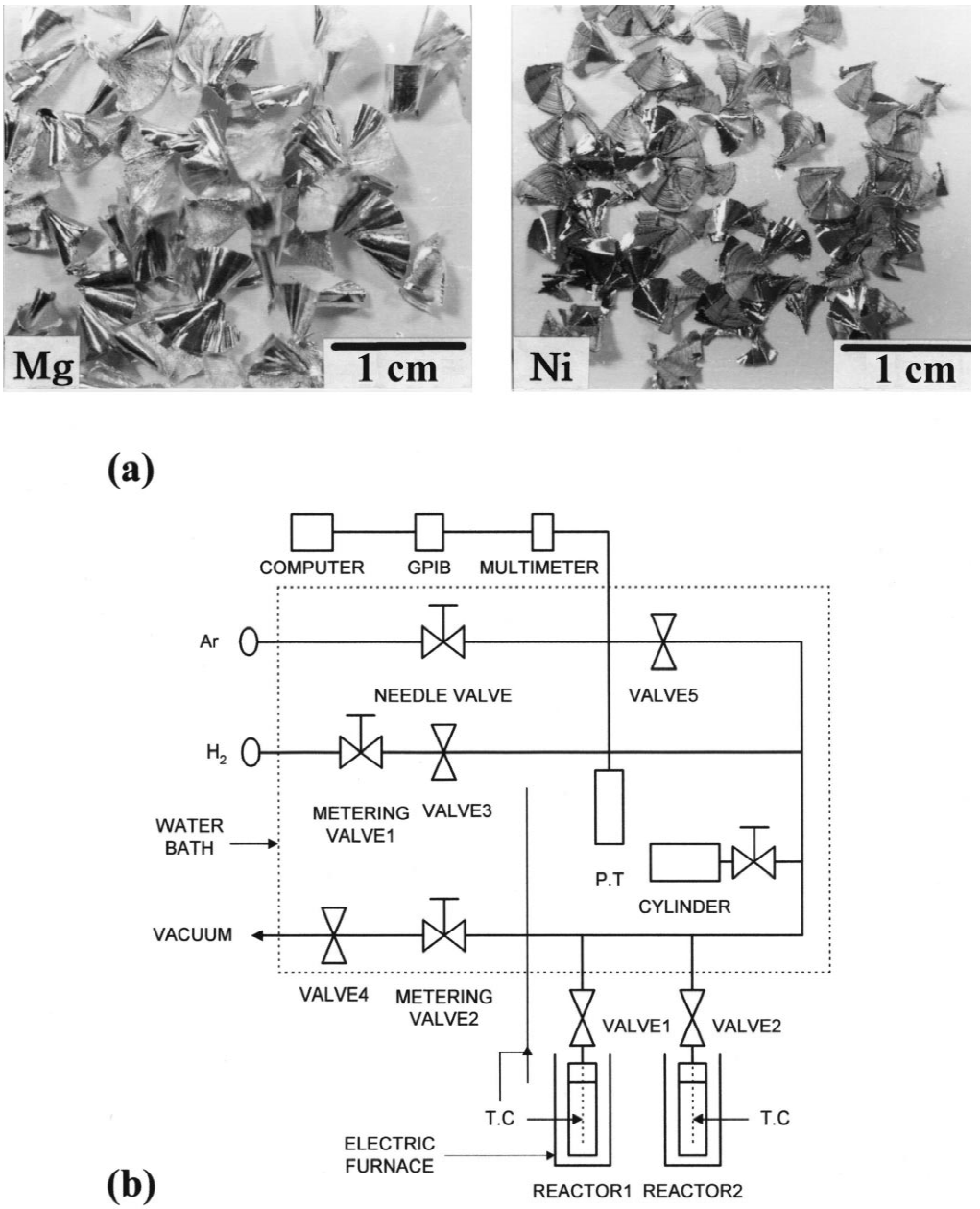

Fig. 1. The shape of Mg and Ni chips (a) and schematic diagram of Sievert's type automatic pressure–composition-isotherm apparatus (b).

volume and 0.5 inch Cr steel balls (AKS Co. Ltd.) were used, and the balls to chips mass ratios (BCR's) were 30:1 and 66:1. After evacuating to 6.7 Pa by rotary pump, the chips were processed by reactive mechanical alloying for 96 h under 2 MPa of high purity hydrogen gas (99.9999%). It was performed by 200 rpm at the ambient temperature using a planetary ball mill (FRITSCH, pulverisette-5).

The MA particles were characterized by X-ray diffraction patterns using a M18XHF-SRA diffractometer (Macscience Co., 1.5405 Å CuKα, 2 deg/min). The morphology of the particles were observed using SEM (JSM-35CF, JEOL Co.) and TEM (HITACHI Co. H-9000-NA).

2.2. Evaluation of the dehydrogenation properties

In order to find the dehydrogenation starting temperature and the phase transition phenomena, thermogravimetry analysis (TGA) was carried out under a pure argon atmosphere with heating to 773 K by 1 K/min. Differential thermal analysis (DTA, SHIMADZU Co. DTA-50) also was carried out from 1 K to 1273 K with the same heating rate as for TGA.

For the calculation of the dehydrogenation reaction enthalpy on synthesized Mg_2NiH_x, isothermal thermogravimetry analysis (ITGA) was carried out under a pure argon atmosphere at 453, 463, 473, 483, 493, 503 and 513 K with holding time for 1 h using TGA-50H (SHIMADZU Co.). Using a Sievert's type automatic PCI apparatus, the hydrogenation/dehydrogenation properties were observed at 393, 423, 453, 483, 513, 543 and 573 K. The schematic diagram of the automatic PCI apparatus was shown in Fig. 1(b).

3. Results and discussion

3.1. The dehydrogenation properties in 30:1 BCR

Fig. 2(a) shows the results of the DTA profiles in 30:1 BCR. The endothermic reactions in stage 1 and 2 are mainly due to the dehydrogenation phenomena and the phase transition, respectively. The hydrogen desorption takes place around 450 K (onset temperature) in stage 1 and the crystal growth and the phase separation proceeds

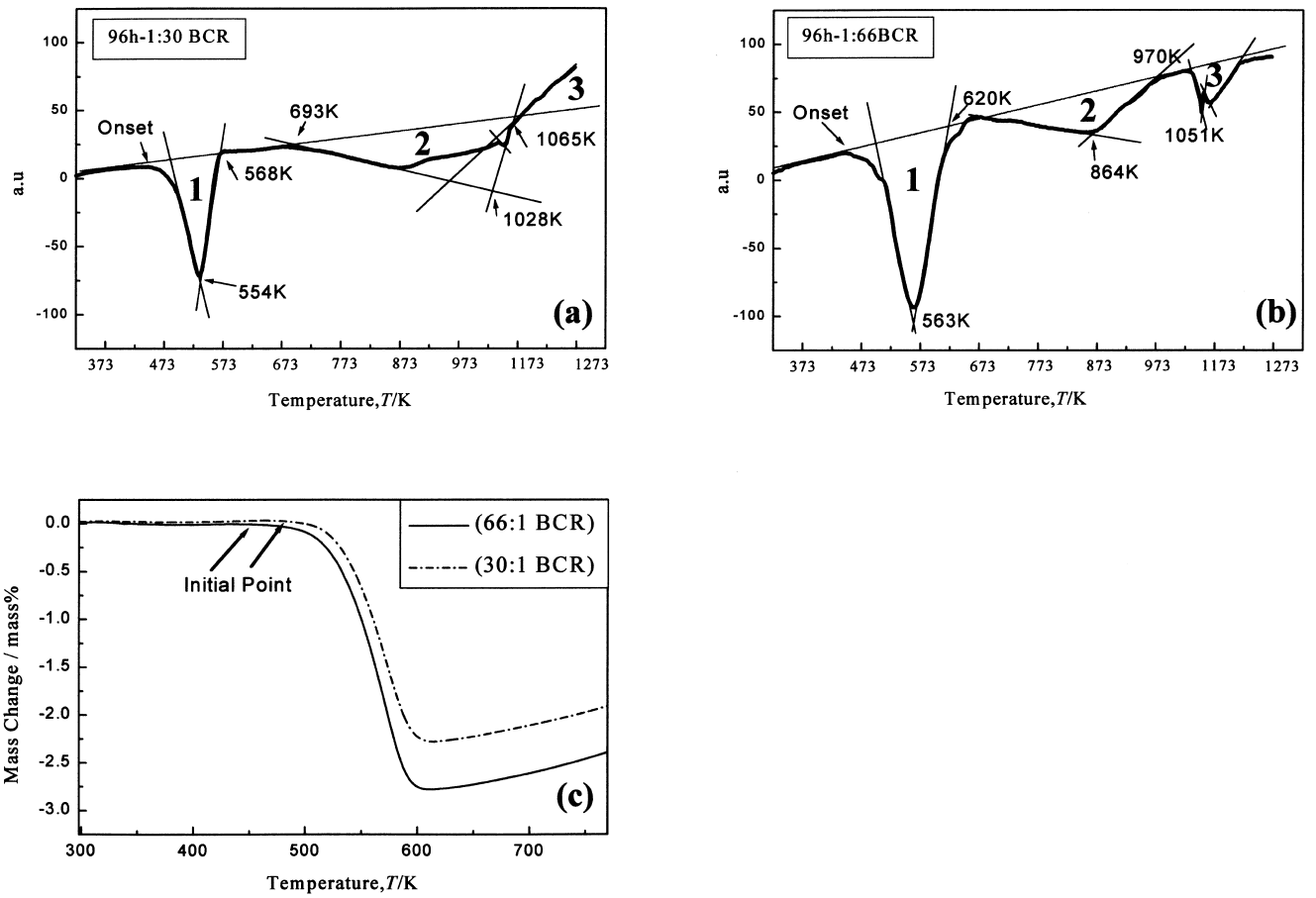

Fig. 2. The results of DTA on MA particles in 30:1 BCR (a), 66:1 BCR (b) and TGA (c). In (c), the arrows indicate the dehydrogenation starting temperature (initial point) about 453, 480 K, respectively.

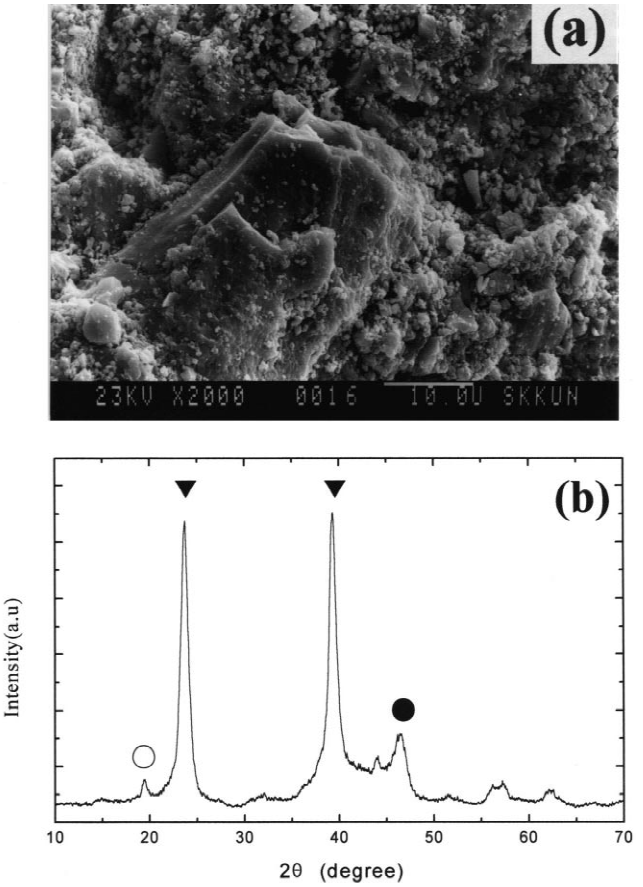

Fig. 3. The morphology of the particles (a) and the XRD patterns (b) in 30:1 BCR. (○: MgH_x, ●: Ni, ▼: Mg_2NiH_x).

in stage 2 [13]. On the other hand, the exothermic reaction in stage 3 seems to occur by the degradation of the particles. The result of TGA in Fig. 2(c) shows that the dehydrogenation temperature starts at about 480 K (initial point) and absorbed hydrogen capacity (AHC) is around 2.25 mass%. The results show that the dehydrogenation temperature is lowered to around 90 K, whereas the value of AHC is decreased by about 1.4 mass% as compared with the fully hydrogenated capacity of polycrystalline Mg_2Ni (3.6 mass% at 572 K) [14]. Fig. 3 shows that the morphology of the particles and the XRD pattern in 30:1 BCR. The fine particles, less than 1 μm, with some porous surface are agglomerated and are composed of a mixture of Mg_2NiH_x, MgH_x and Ni. The retained Ni, which is seen in the early MA stage, is caused by the formation of MgH_x [15]. From the typical bright field image and the corresponding selected area diffraction (SAD) pattern of Mg_2NiH_x (Fig. 4), reveal that the average crystal size is less than 50 nm and the nanocrystalline and amorphous phases coexist. In Fig. 5, the result of ITGA and the calculated Arrhenius plot indicate that the hydrogenation reaction dose not proceed for 1 h below 453 K, but the dehydrogenation proceeds over 503 K, and the activation energy is estimated to be 51.6 ± 2.1 kJ/mol H_2 by the linear fit of the Arrhenius plot within the range from 0.5 to 1 ks. The dehydrogenation behaviors of PCI and the corresponding van't Hoff plot in Fig. 6 show that the calculated $\Delta_r H^0$ is about 81.1 ± 0.2 kJ/mol H_2 except the case of the dehydrogenation reactions at 483 K.

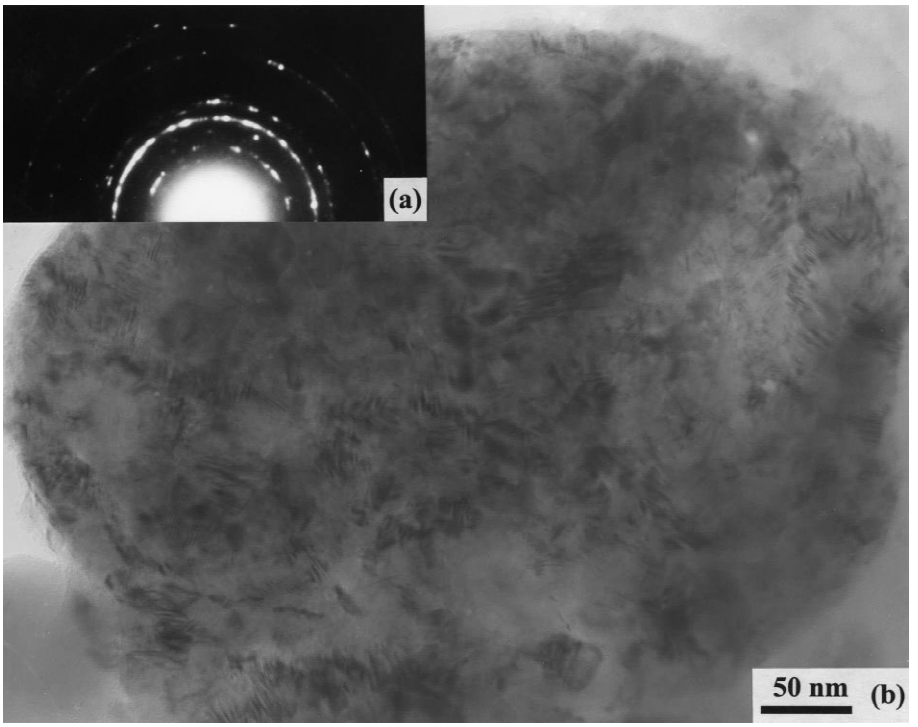

Fig. 4. The SAD pattern (a) and the bright field image (b) of the Mg_2NiH_x particles after 96 h MA in 30:1 BCR.

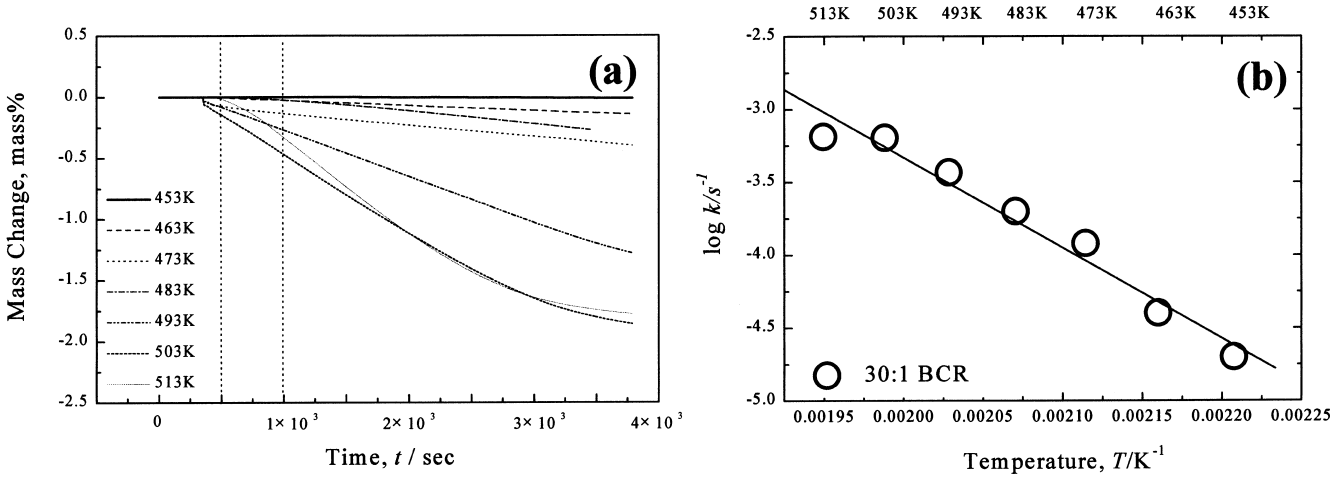

Fig. 5. The profiles of ITGA (a) and the Arrhenius plot (b) from 0.5 to 1.0 ks in 30:1 BCR.

3.2. The dehydrogenation properties in 66:1 BCR

Fig. 2(b) shows the results of the DTA profiles in 66:1 BCR. The endothermic reactions in stage 1 and 2 are by the dehydrogenation reactions (onset temperature around 440 K) and the coarsening of the nanocrystalline Mg_2Ni, respectively. The endothermic reaction in stage 3 is caused by the phase separation of the Mg_2Ni and the hydrogen desorption initial temperature indicated at around 453 K in Fig. 2(c). These results demonstrate that the Mg_2NiH_x particles synthesized in 66:1 BCR show more stable behaviors compared with those in 30:1 BCR. Even though the dehydrogenation starting temperature is poorer, about 13 K, than Orimo et al. [16], the value of AHC, around 2.80 mass%, is larger than their achievement, 1.6 mass% [16,17]. These results are caused by the synthesized phase of various hydrides via MA. In other words, the difference of hydrogen capacity between LT–Mg_2NiH_4 and $Mg_2NiH_{1.8}$ is affected by the dehydriding temperature and the AHC. Fig. 7 shows the morphology of the particles and the XRD patterns in 66:1 BCR. The Mg_2NiH_4, a little Ni is detected with small MgH_x, and nanocrystalline particles, less than 1 μm, with a high porous surface are observed in comparison with those of 30:1 BCR. Fig. 8 shows the microstructure of the particles after 96 h MA in 66:1 BCR. The average grain size is measured at less than 10 nm from the bright field image and the particles are composed of the nanocrystalline and amorphous phases. The corresponding SAD patterns of the Mg_2NiH_x show the continuous and broaden ring pattern, which indicates the coexistence of the homogeneously distributed amorphous and the fine nanocrystalline phases. According to Fujii et al. [18] and Yamamoto et al. [19], these phases was considered to be affirmative factors of dehydrogenation reaction kinetics such as ‘cooperative dehydriding phenomena’. Fig. 9 shows the results of ITGA and the Arrhenius plot in 66:1

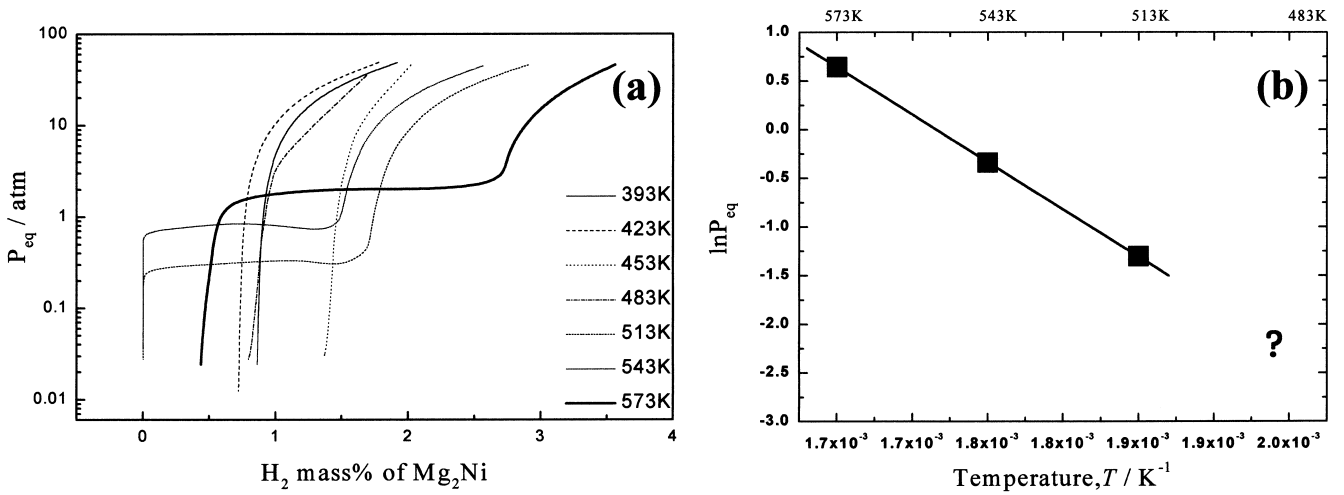

Fig. 6. The PCI profiles of the dehydriding reactions (a) and the van’t Hoff plot (b) from 513 to 573 K in 30:1 BCR.

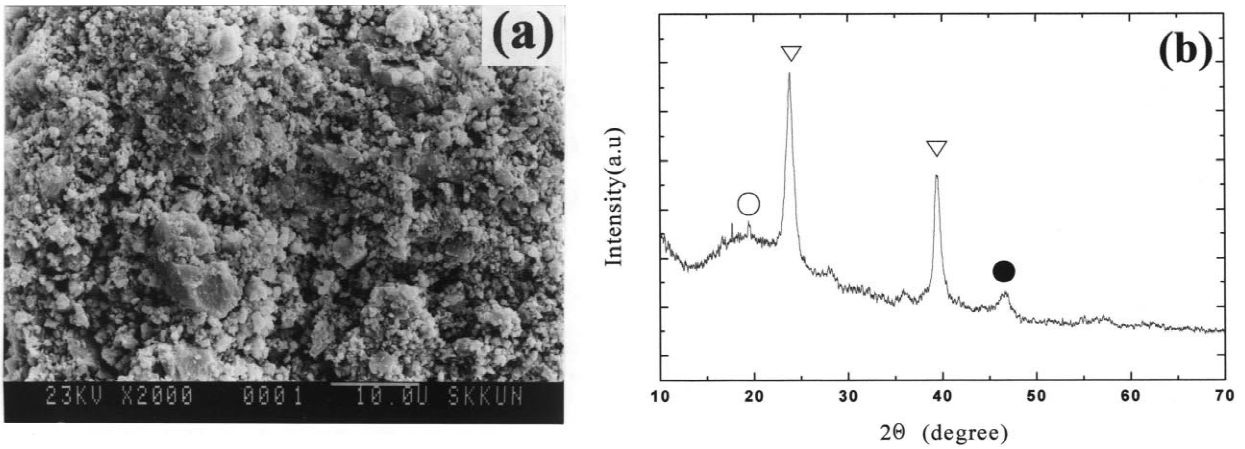

Fig. 7. The morphology of the particles (a) and the XRD patterns (b) in 66:1 BCR. (○: MgH_x, ●: Ni, ▽: Mg_2NiH_4).

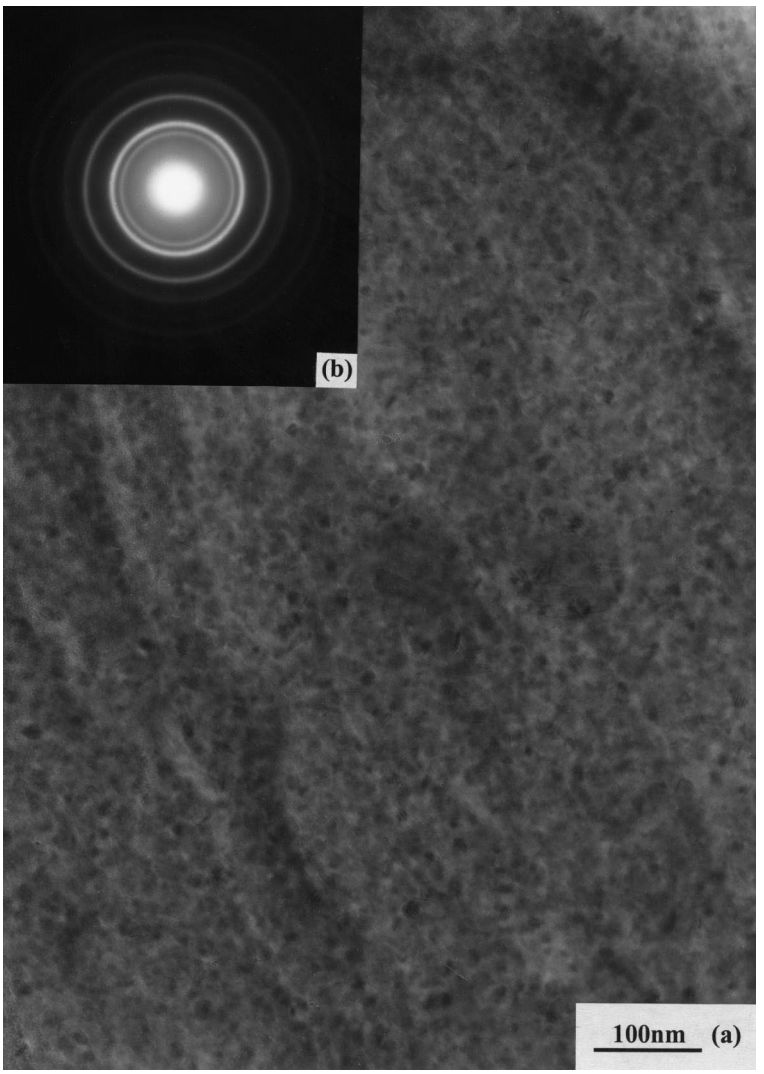

Fig. 8. The brightfield image of the Mg_2NiH_x particles after 96 h MA in 66:1 BCR (a) and the SAD pattern (b) shows the continuous and broaden ring patterns.

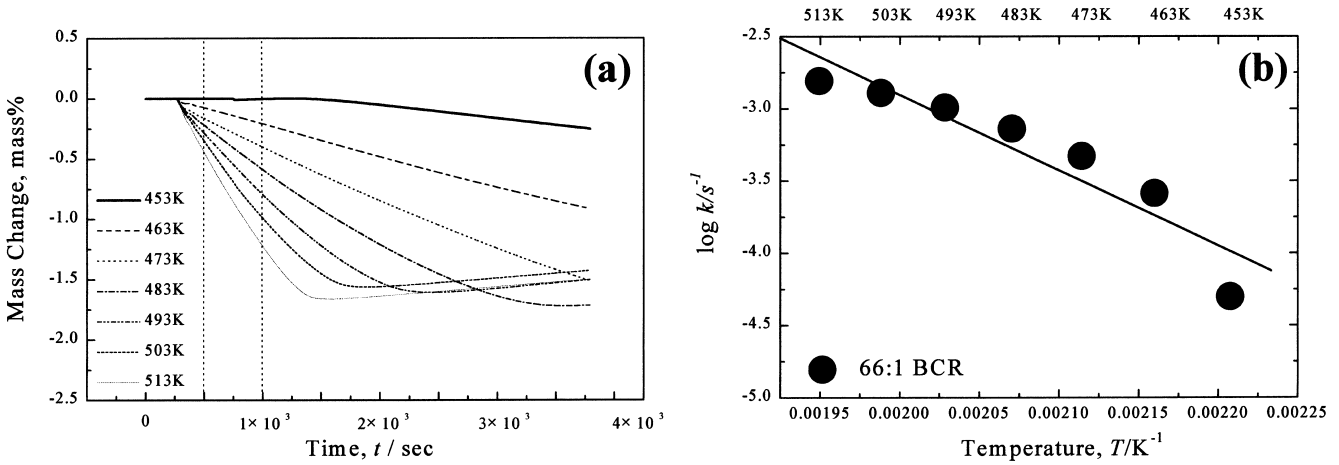

Fig. 9. The profiles of ITGA (a) and the Arrhenius plot (b) from 0.5 to 1.0 ks in 66:1 BCR.

BCR. The dehydrogenation reaction proceeds for 1 h at 453 K slowly, but at over 473 K the dehydrogenation reaction is completely established. The activation energy is estimated to be 43.4±3.6 kJ/mol H_2 by the linear fit of the Arrhenius plot with the range from 0.5 to 1 ks. Fig. 10 shows the data of PCI on the Mg_2Ni, which treated of initial dehydrogenation without activation. The PCI curve at 483 K shows the dehydrogenation plateau pressure at 0.01 MPa without the entrapped hydrogen. The plateau slope of about 0.05, the hysteresis of about 0.94, the hydrogen capacity of about 2.25 mass% and the reversible capacity of 1.08 mass% are observed by the PCI curves. From the van't Hoff plot, the calculated dehydrogenation reaction enthalpy, $\Delta_r H^0$ is about 91.4±0.9 kJ/mol H_2. By comparing the properties between 30:1 and 66:1 BCR, the Mg_2Ni particles in 66:1 BCR might be better candidate materials for hydrogen storage applications.

4. Conclusions

Mg_2NiH_x composed of the nanocrystalline and the amorphous phases are synthesized successfully by hydrogen induced mechanical alloying from Mg and Ni chips. The BCR conditions mainly affect the hydrogenation properties due to the formation of the Mg_2NiH_x. The maximum AHC is 2.8 mass% after 96 h MA in 66:1 BCR and the hydrogen capacity of the nanocrystalline and amorphous phases is about 2.25 mass% at 483 K from PCI analysis. The dehydrogenation properties are mainly dependent on the microstructure of the particles. In such a way that the properties were better in the case of 66:1 BCR. The crystal structure modification to nanocrystalline with the amorphous phase for controlling Mg_2NiH_x by hydrogen induced mechanical alloying might be one of the reasonable solutions for manufacturing Mg_2NiH_x hydrogen

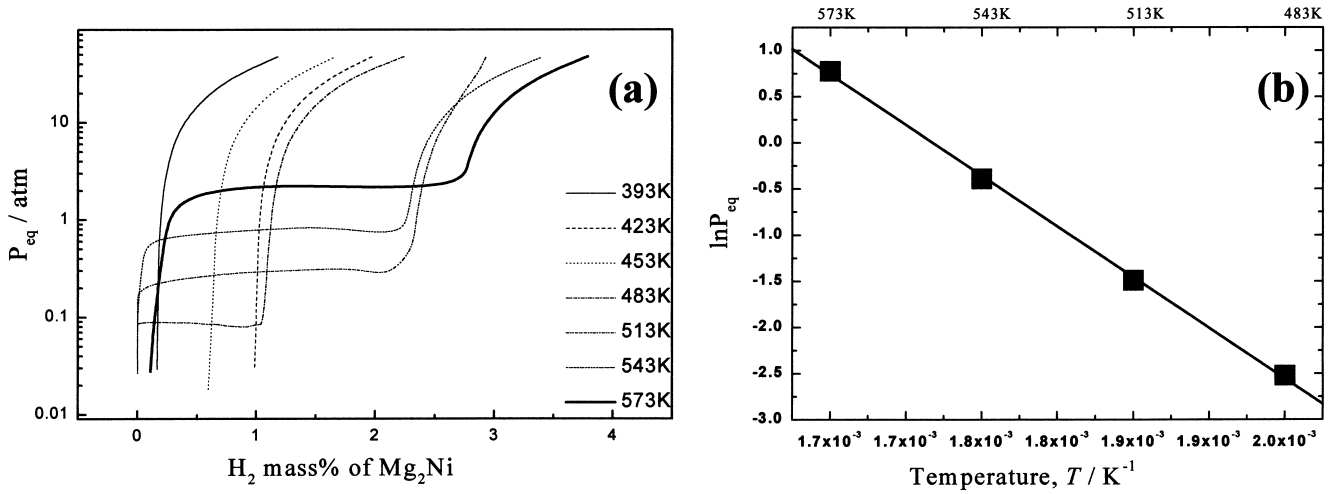

Fig. 10. The PCI profiles of the dehydriding reactions (a) and the van't Hoff plot (b) from 483 to 573 K in 66:1 BCR.

storage materials and improving their dehydrogenation properties.

References

[1] R.W. Chan, P. Haasen (Eds.), Physical Metallurgy, 4th Edition, North Holland, 1996, p. 900.
[2] E. Arzt, L. Schultz (Eds.), New Materials by Mechanical Alloying Techniques, Informations Gesellschaft Verlag, 1989, p. 307.
[3] H.W. Schufer, R. Wurschum, J. Less-Common Met. 140 (1988) 161.
[4] L. Schlapbach (Ed.), Hydrogen in Intermetallic Compounds II, Springer Verlag, 1992, p. 178.
[5] M.Y. Song, E.I. Ivanov, B. Darriet, M. Pezat, P. Hagenmuller, Int. J. Hydrog. Ener. 10 (1985) 169.
[6] L. Zaluski, A. Zaluska, J.O. Ström-Olsen, J. Alloys Comp. 253–254 (1997) 70.
[7] J. Hout, E. Akiba, T. Takaba, J. Alloys Comp. 231 (1996) 815.
[8] S. Orimo, H. Fujii, J. Alloys Comp. 232 (1996) 116.
[9] R.L. Holtz, M.A. Imam, J. Mater. Sci. 32 (1997) 2267.
[10] F.J. Liu, S. Suda, J. Alloys Comp. 232 (1996) 212.
[11] T.W. Hong, S.K. Kim, G.S. Park, Y.J. Kim, Mater. Trans., JIM 41 (2000) 393.
[12] T.W. Hong, J.W. Lim, S.K. Kim, Y.J. Kim, H.S. Park, J. Kor. Inst. Met. Mater. 37 (1999) 369, in Korean.
[13] M.Y. Song, J. Alloys Comp. 282 (1999) 297.
[14] J.J. Reilly, R.H. Wiswall, Inorg. Chem. 7 (1968) 2254.
[15] T.W. Hong, J.W. Lim, S.K. Kim, Y.J. Kim, H.S. Park, J. Kor. Hydrog. Ener. Soc. 10 (1999) 27, in Korean.
[16] S. Orimo, H. Fujii, K. Ikeda, Y. Kitano, J. Jap. Inst. 60 (1996) 685, in Japaness.
[17] S. Orimo, H. Fujii, J. Alloys Comp. 232 (1996) L16.
[18] H. Fujii, S. Orimo, K. Ikeda, J. Alloys Comp. 253–254 (1997) 80.
[19] K.-i. Yamamoto, Y. Fujikawa, K. Ikeda, S.-i. Orimo, H. Fujii, Y. Kitano, J. Electron Microsc. 47 (1998) 461.